Individual Extraction of Street Trees From MLS Point Clouds Based on Tree Nonphotosynthetic Components Clustering

Jintao Li, Hangbin Wu, Xiaolong Cheng, Yuanhang Kong, Xufei Wang, Yanyi Li, and Chun Liu, *Member, IEEE*

***Abstract*—The individual extraction of street trees from mobile laser point clouds is the prerequisite for their digital expression and application. However, due to the complexity of urban road environment and the diversity of street trees, especially the scenes where adjacent trees are different in type, size, and crown overlap, accurate extraction of individual street trees is still difficult to achieve. Therefore, in this article, a new method to extract street trees individually from mobile laser scanning point clouds is proposed. First, the ground and buildings are removed through data preprocessing. Then, the artificial poles that may overlap with street tree crowns are further removed by supervoxels region growing, and the regions of interest (ROI) including street trees and understory vegetation are selected. After that, the main branch part (including trunk) of each tree is separated from the ROI by nonphotosynthetic components clustering. Finally, based on the individual clustering results of nonphotosynthetic components, the remaining photosynthetic components in the ROI are segmented individually, and the vegetation under the tree is removed through gradual refinement to achieve the complete segmentation of individual trees. An urban area with a total road length of more than 2.1 km, including six roads with different complexity, was used to verify the effectiveness of the proposed method for the individual extraction of street trees. The results show that the proposed method can be effectively used for individual extraction of street trees in different complexity scenes. Overall, the precision, recall and F-score of street tree individual extraction are 94.5%, 97.4%, and 95.9%, respectively.**

***Index Terms*—Clustering, mobile laser scanning (MLS) point cloud, road environment, street tree extraction, tree nonphotosynthetic components.**

Manuscript received 12 February 2023; revised 10 April 2023; accepted 29 May 2023. Date of publication 1 June 2023; date of current version 14 June 2023. This work was supported in part by the National Major Science and Technology Projects of China under Grant 2021YFB2501103, in part by the National Natural Science Foundation of China under Grants 42271429 and 42004158. *(Corresponding author: Hangbin Wu.)*

Jintao Li, Yuanhang Kong, and Yanyi Li are with the College of Surveying and Geo-Informatics, Tongji University, Shanghai 200092, China (e-mail: lijintao@tongji.edu.cn; 2111330@tongji.edu.cn; 2131939@tongji.edu.cn).

Hangbin Wu and Chun Liu are with the College of Surveying and Geo-Informatics, Urban Mobility Institute, Tongji University, Shanghai 200092, China (e-mail: hb@tongji.edu.cn; liuchun@tongji.edu.cn).

Xiaolong Cheng is with the College of Civil and Surveying and Mapping Engineering, Jiangxi University of Science and Technology, Ganzhou 341000, China (e-mail: chengxiaolong@jxust.edu.cn).

Xufei Wang is with the Shanghai Research Institute for Intelligent Autonomous Systems, Tongji University, Shanghai 200092, China (e-mail: tjwangxufei@tongji.edu.cn).

Digital Object Identifier 10.1109/JSTARS.2023.3281787

I Introduction

As a large proportion of urban features, street trees are an important part of digital city construction and city information model (CIM) building. The development of three-dimensional (3-D) laser scanning, especially the mobile laser scanning (MLS) technology, provides a data basis for the accurate and detailed 3-D expression of street trees [1], [2], [3]. Individual extraction of street trees from scattered and disordered laser point clouds is the prerequisite for their expression and application.

Different from forest scenes that do not contain various man-made objects, the focus of individual extraction of street trees from road scenes is to accurately identify and distinguish tree trunks and artificial pole-like objects, and reasonably segment the overlapping parts of tree crowns. Individual extraction methods for forest trees based on trunk or treetop detection [4], [5], such as the trunk detection via cylinder fitting and treetop detection via local highest point finding, cannot be applied directly to street trees. In recent years, many street tree individual extraction methods orient to MLS point clouds have been proposed. According to the different extraction strategies, these methods can be divided into classification based methods [6], [7], [8], [9], top-down segmentation methods [10], [11], [12], and bottom-up segmentation methods [13], [14], [15], [16], [17]. In the classification based methods, the raw point cloud is first classified by machine learning or deep learning, and then the tree points obtained by classification are individually segmented via certain segmentation or clustering algorithms (e.g., graph based segmentation [7] and mean shift based clustering [8]). Both top-down and bottom-up segmentation methods first remove the easily identifiable non-tree objects (such as ground) via simple data preprocessing, and then segment the street tree individuals from the remaining objects through different strategies. The top-down strategy is to cluster the remaining objects into many large segments by Euclidean distance at first, then identify and select the segments containing trees according to their global characteristics (e.g., size, height, and shape), and remove the mixed nontree objects (e.g., street lights and traffic signs) to obtain tree individuals through some segmentation method (e.g., voxel-based normalization cut [10] and coarse-to-fine segmentation method [11]). Compared with the method of classifying trees first and then segmenting them individually,

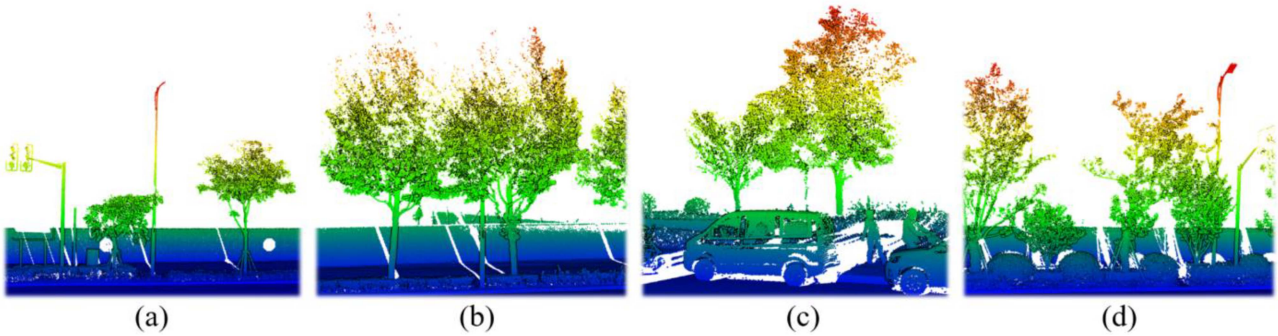

Fig. 1. Common street tree scenes. (a) Common scene 1, little or no overlap between adjacent trees and between tree crowns and artificial pole-like objects. (b) Common scene 2, large overlap between adjacent trees and between tree crowns and artificial pole-like objects. (c) Common scene 3, tree trunks are partially or completely missing due to occlusion. (d) Common scene 4, shape, size and type of adjacent trees vary greatly, some trees have no obvious trunks, and there are overlaps between tree crowns and between tree crowns and artificial pole-like objects.

this method of separating trees individually from objects containing nontrees has higher requirements of the segmentation algorithms. The bottom-up strategy first identifies and locates the tree positions (represented by tree trunk [13], [14], [15], tree trunk and branches [16], or the junction of trunk and branches [17]) through local features from the remaining objects after preprocessing, and then individually segments the tree points via location-based region growing [13], [14], [15] or clustering [16], [17].

Different street tree individual extraction methods have their own applicable scenes. We categorize common street tree scenes into four types (see Fig. 1) based on the overlap between tree individuals and their adjacent objects (adjacent trees and artificial pole-like objects), as well as tree shape characteristics (differences in size and shape of crown and trunk integrity in MLS points). These include: common Scene 1, where the spacing between trees is large and there is little or no overlap between trees and artificial pole-like objects; common Scene 2, where the overlap between tree crowns is large and the artificial pole-like objects and trees also overlap greatly; common Scene 3, where the tree trunks are partially or completely missing due to the occlusion of other objects such as vehicles and green belts; common Scene 4, where the shape, size and type of adjacent trees vary greatly, there are trees without obvious trunks, and overlaps also occur between tree crowns and between tree crowns and artificial pole-like objects. For common Scene 1, since this scene is simple and the geometric characteristics of trees and artificial pole-like objects are obvious and easy to be distinguished, the existing classification based methods, top-down and bottom-up segmentation methods can all accurately extract the street tree individuals in it. For common Scene 2 where there are serious overlaps between trees and artificial pole-like objects, the applicability of the classification based method is not satisfactory because the existing classification methods cannot accurately distinguish the tree trunks and artificial vertical poles in this scene. According to Luo et al. [18], the mIoU of the best classification results of the existing deep learning methods for artificial pole-like objects and trees are only 79.7% and 91.4%, respectively. From Weinmann et al. [19], existing machine learning cannot distinguish between tree trunks and artificial vertical poles, and as the same category, their classification precision and recall are only 34.7% and 82.1%, respectively. The presence of artificial pole-like objects in the tree crown, which lack distinct shape differences from trees, makes it challenging for existing top-down segmentation methods to accurately identify and segment them. In the bottom-up segmentation methods, the methods based on tree trunk recognition to locate tree positions are easy to misidentify artificial vertical poles as tree trunks in common Scene 2, thus affecting the results of individual tree segmentation. The method based on branch and trunk matching [17] can effectively identify the tree positions and can be used in common Scene 2. For common Scene 3 with missing or incomplete tree trunks, the bottom-up segmentation methods are prone to missed extraction because the tree positions cannot be identified, and the classification based or top-down segmentation methods can achieve individual extraction of street trees in this scene when there is small difference in tree size and there is little overlap between trees and artificial pole-like objects. For complex common Scene 4, the existing bottom-up segmentation methods cannot locate trees without obvious trunks, the existing top-down segmentation methods cannot accurately identify and segment the Euclidean-clustered tree segments with large differences in tree size, shape and crown overlap, and the classification based methods do not apply well because of the scene complexity. To sum up, the existing methods for street trees individual extraction from MLS point clouds are not universal enough to be competent for the four common road scenes. In addition, there is a lack of street tree individual extraction methods that can be applied to the complex road scene as shown in common street tree Scene 4.

To achieve individual extraction of street trees from various common road scenes, in this article, a new method based on non-photosynthetic components clustering is proposed for the individual extraction of street trees from MLS point clouds. The main contributions include: 1) a tree nonphotosynthetic components clustering method based on intensity and density of laser point is proposed, which can effectively identify the basic shape of each street tree and locate its position, including small trees without obvious trunks; and 2) a complete individual tree segmentation method based on nonphotosynthetic components and gradual refinement of understory vegetation is proposed, which can effectively segment tree individuals

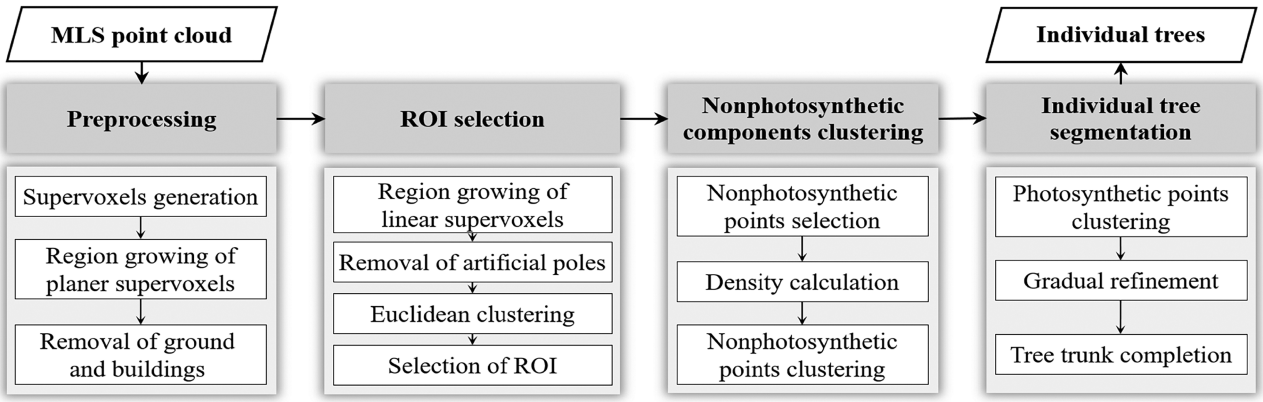

Fig. 2. Technical flowchart of the proposed method.

with large differences in shape, size, and crown overlap, and the understory vegetation and trunk holders can be effectively removed in the segmentation results. The proposed method has strong universality and is competent for different common road scenes.

The rest of this article is organized as follows. We begin with a detailed introduction of the proposed street tree individual extraction method (see Section II). We then outline the experimental data and the implementation of method validation (see Section III), and discuss the effectiveness and advantages of the proposed method (see Section IV). Finally, Section V concludes this article.

II. Method

The proposed method mainly includes four processes (see Fig. 2): 1) data preprocessing, 2) regions of interest (ROI) selection, 3) street tree nonphotosynthetic components clustering, and 4) street tree individual segmentation. In data preprocessing, ground and buildings are removed. Then, the artificial poles that may overlap with tree crowns are identified and further removed, and the ROI including street trees and understory vegetation are selected. After that, the nonphotosynthetic components in the ROI are extracted and clustered to achieve individual separation of main branch part (including trunk) of each tree. Finally, based on the individual clustering results of nonphotosynthetic components, the remaining photosynthesis components in the ROI are segmented individually, the understory vegetation and trunk holders are removed through gradual refinement, and the individual trees are extracted after trunk completion.

A. Data Preprocessing

The purpose of data preprocessing is to remove the ground and buildings that account for a large proportion of the raw MLS point clouds. These objects usually connect with different objects and occupy large storage space [12], [20], [21]. Their removal can effectively reduce the complexity of data processing and improve the efficiency of street tree individual extraction. Here, the supervoxel-based region growing method proposed by Li et al. [22] is used to remove the ground and buildings. First, the raw point cloud [see Fig. 3(a)] is supervoxelized with boundary preservation of different objects [see Fig. 3(b)]. Then, the dimensional feature of each supervoxel is judged by principal component analysis (PCA) [23], and nonvolumetric supervoxels are taken as planer supervoxels to perform region growing [see Fig. 3(c)]. Finally, the planar patch with a certain area and normal direction parallel to the Z-axis is selected as the ground [gray part in Fig. 3(d)], and the planar patches with certain areas and normal directions perpendicular to the ground are selected as building facades, and the buildings [see red parts in Fig. 3(d)] are identified through facade occlusion analysis [22]. The result after preprocessing is shown in Fig. 3(e).

The specific PCA-based supervoxel dimensional feature judgment method is as follows. Let $\{ p_1, p_2, \ldots p_k \}$ be the point set in one supervoxel, and a_L, a_P, a_V represent the degree of linear, planer and volumetric of the supervoxel, respectively. Their calculation is

$$\left.\begin{aligned} a_L &= \frac{\sqrt{\lambda_1}-\sqrt{\lambda_2}}{\sqrt{\lambda_1}} \\ a_P &= \frac{\sqrt{\lambda_2}-\sqrt{\lambda_3}}{\sqrt{\lambda_1}} \\ a_V &= \frac{\sqrt{\lambda_3}}{\sqrt{\lambda_1}} \end{aligned}\right\} \tag{1}$$

$$\boldsymbol{M} = \frac{1}{k}\sum_{i=1}^{k}(p_i-\bar{p})\cdot(p_i-\bar{p})^T \tag{2}$$

where λ_1, λ_2, λ_3 $(\lambda_1 \geq \lambda_2 \geq \lambda_3)$ is the eigenvalues of the covariance matrix $\boldsymbol{M}$ of the supervoxel point set, and $\bar{p} = \frac{1}{k}\sum_{i=1}^{k} p_i$. The feature corresponding to the largest of a_L, a_P, and a_V is the dimensional feature of the supervoxel.

B. ROI Selection

We further select the ROI that only contain trees and understory vegetation as much as possible from the preprocessing result to narrow the area where street trees are located. Without the ground and buildings as connectors, most of the nontree objects after preprocessing are usually dispersed and independent [as shown in Fig. 3(e)], except that some artificial pole-like objects may be overlapped in the tree crowns or connected with street trees through the understory vegetation. In order to remove the artificial pole-like objects overlapped with street trees, we first reidentify the linear supervoxels from the preprocessing result [see Fig. 4(a)] based on PCA, and grow

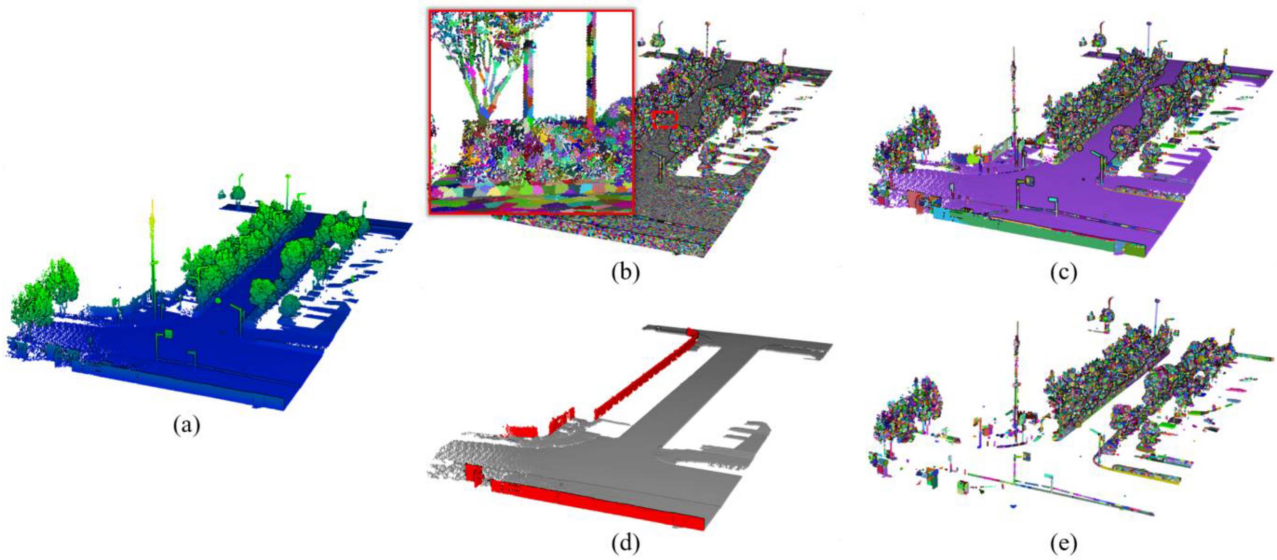

Fig. 3. Data preprocessing based on supervoxels region growing. (a) Raw point cloud (colored by elevation). (b) Supervoxelization (different colors represent different supervoxel individuals). (c) Region growing result of nonvolumetric supervoxels (distinguished by colors). (d) Extracted ground (grey) and buildings (red). (e) Preprocessing result expressed by supervoxels.

the adjacent linear supervoxels with similar principal directions (intersection angle less than 10°). At this time, the vertical and horizontal poles of the artificial pole-like objects are divided into independent parts with obvious boundaries with the surrounding objects, as shown in Fig. 4(b). However, a vertical pole may be divided into multiple segments due to crown occlusion and the influence of attachments on the vertical pole. Then, we merge the vertical pole segments more than a certain length (1.0 m) and close to each other in horizontal (horizontal distance between the two centers is less than 0.2 m) to optimize the linear supervoxels growing results. After optimization, each artificial vertical pole is divided into an independent individual. Since the artificial vertical poles usually higher than tree trunks and the artificial horizontal poles usually located at the upper end of the artificial vertical poles, they can be identified [see Fig. 4(c)] and removed according to the length and height characteristics. After the removal of the artificial poles, there are spatial separations between the artificial pole attachments and the tree crowns [see Fig. 4(d)]. We cluster the remaining objects into many clusters based on spatial connectivity through Euclidean clustering, and select the ROI from them according to the principle that the clusters including street trees are usually large in size. For areas with many dense vegetation under the tree, we also remove the non-street tree points close to the ground to further narrow the ROI. The finally selected ROI is, as shown in Fig. 4(e).

C. Nonphotosynthetic Components Clustering

Although the artificial pole-like objects in the ROI have been removed, the existing methods are still difficult to achieve accurate segmentation of individual street trees in the scenes with large differences in tree types, unclear boundaries of adjacent crowns, and unobvious or missing tree trunks. To overcome the shortcomings of the existing methods for identifying and locating street trees based on tree trunks, we propose an individual clustering method of tree nonphotosynthetic components based on the intensity and local density characteristics of point clouds, and use the nonphotosynthetic components clustering results to identify and locate each street tree.

In the laser point cloud data, in addition to 3-D coordinates, each laser point usually has an intensity attribute mainly related to the reflection characteristics of the object surface [24]. Although the intensity value is also affected by the scanning distance and scanning angle [25], our research objects are street trees, which are mostly arranged on both sides of the road in parallel and have a small range of variation in scanning distance and scanning angle in the MLS point cloud. In addition, due to the complexity of objects in the road environment, few studies on MLS have investigated the intensity correction [24]. The existing applications that use MLS intensity do not address intensity correction (such as [26], [27], [28], [29]). From the ROI colored by intensity in Fig. 5(b), it can be seen that the original uncorrected intensities have obvious differences between nonphotosynthetic and photosynthetic components, which allows them to be roughly distinguished by a threshold. Therefore, we first select the points whose intensity is greater than the specified threshold T_{inten} as the nonphotosynthetic component points of trees. Then, we calculate the local density of each point in the nonphotosynthetic components. The local density of a point p is inversely proportional to the average point spacing of its k-nearest neighbors, as expressed as follows:

$$D^p = \frac{k}{\sum_{i=1}^{k} ||p - p_i||}. \tag{3}$$

As shown in Fig. 5(c), although the values of the maximum local density vary greatly among different trees, these maximum local densities are all located on the main branch part (including trunks) of each tree, so the position of each tree can be detected based on the spatial variation of the local density of nonphotosynthetic components.

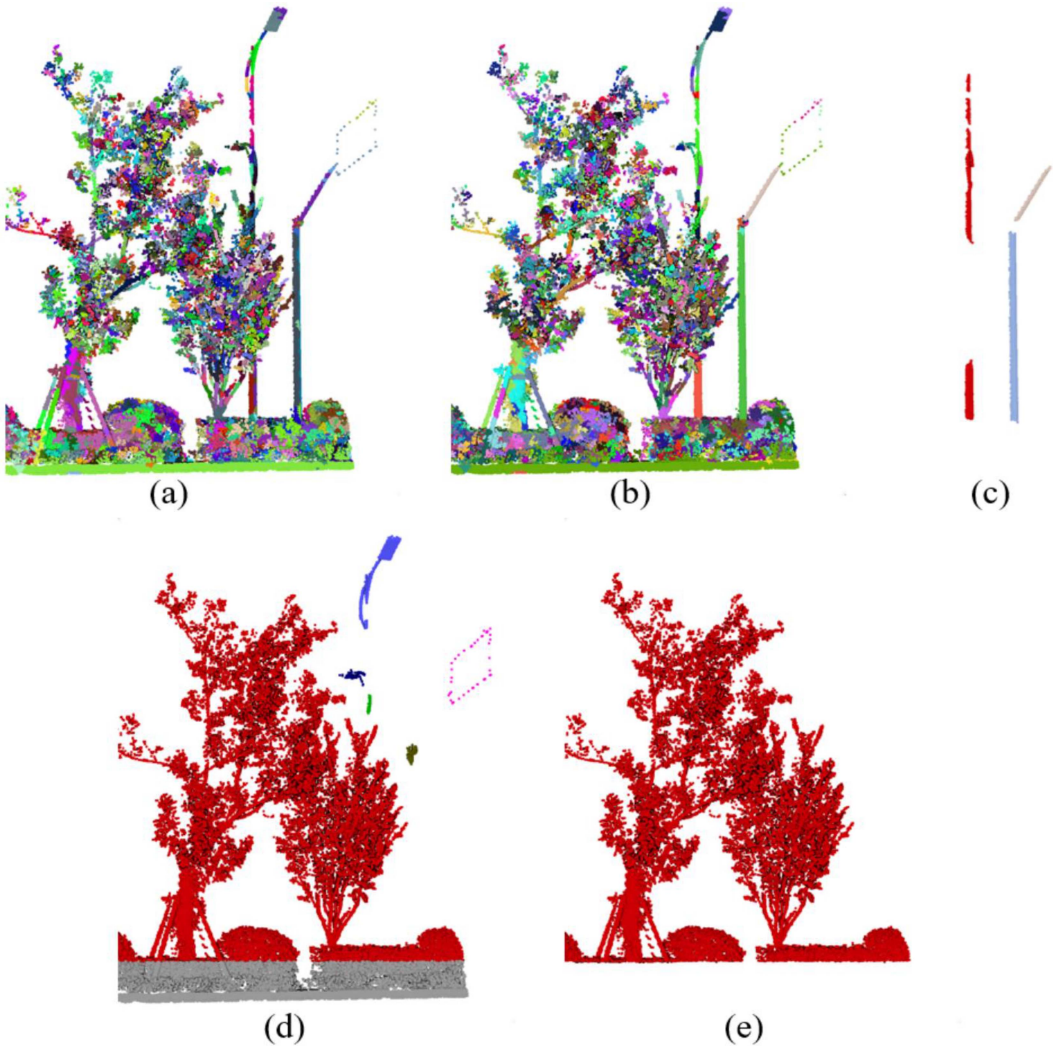

Fig. 4. ROI selection. (a) Preprocessing result expressed by supervoxels. (b) Region growing result of linear supervoxels (distinguished by colors). (c) Extracted artificial poles (including vertical and horizontal poles). (d) Euclidean clustering result (distinguished by colors). (e) Selected ROI.

In order to individually separate the nonphotosynthetic components of different trees while determining the tree positions, we cluster each nonphotosynthetic point in turn according to the order of local density from small to large. Specifically, for a point P_i, find the point P_j that is closest to P_i and whose local density is greater than P_i, then calculate the horizontal distance $D_{i,j}^{xy}$ between P_i and P_j, if $D_{i,j}^{xy} < T_{\text{dis}}$, P_i is clustered into P_j to generate a cluster represented by P_j. The horizontal distance threshold T_{dis} can be taken as a value that is slightly less than the street tree spacing

$$D_{i,j}^{xy} = \sqrt{(P_{ix} - P_{jx})^2 + (P_{iy} - P_{jy})^2} \ . \tag{4}$$

After clustering, nonphotosynthetic points belonging to the same tree are clustered together, as shown in Fig. 5(d). The detailed process of extraction and clustering of nonphotosynthetic components is shown in Fig. 6.

D. Individual Tree Segmentation

To achieve the individual segmentation of street trees, based on the clustering results of nonphotosynthetic components, we determine the cluster category of each separated photosynthetic component point according to the order of elevation from small to large. The cluster category of a photosynthetic component point P_i is the same as that of P_j, which is the closest to P_i among the clustered nonphotosynthetic components. After the category of P_i is determined, add it to the corresponding cluster and update the clustering result. As shown in Fig. 7(a), the ROI segmentation result with proper individual crown boundaries can be obtained.

Affected by the understory vegetation and the trunk holders, each separated individual tree contains nontree components [see Fig. 7(a)]. Here, these nontree components are gradually removed by iterative slicing. As shown in Fig. 8(a), for the segmentation result of each tree, starting from the 1/2 height of the tree, slice downward along the Z-axis at an interval of 0.1 m, and calculate the length and center of the bounding box

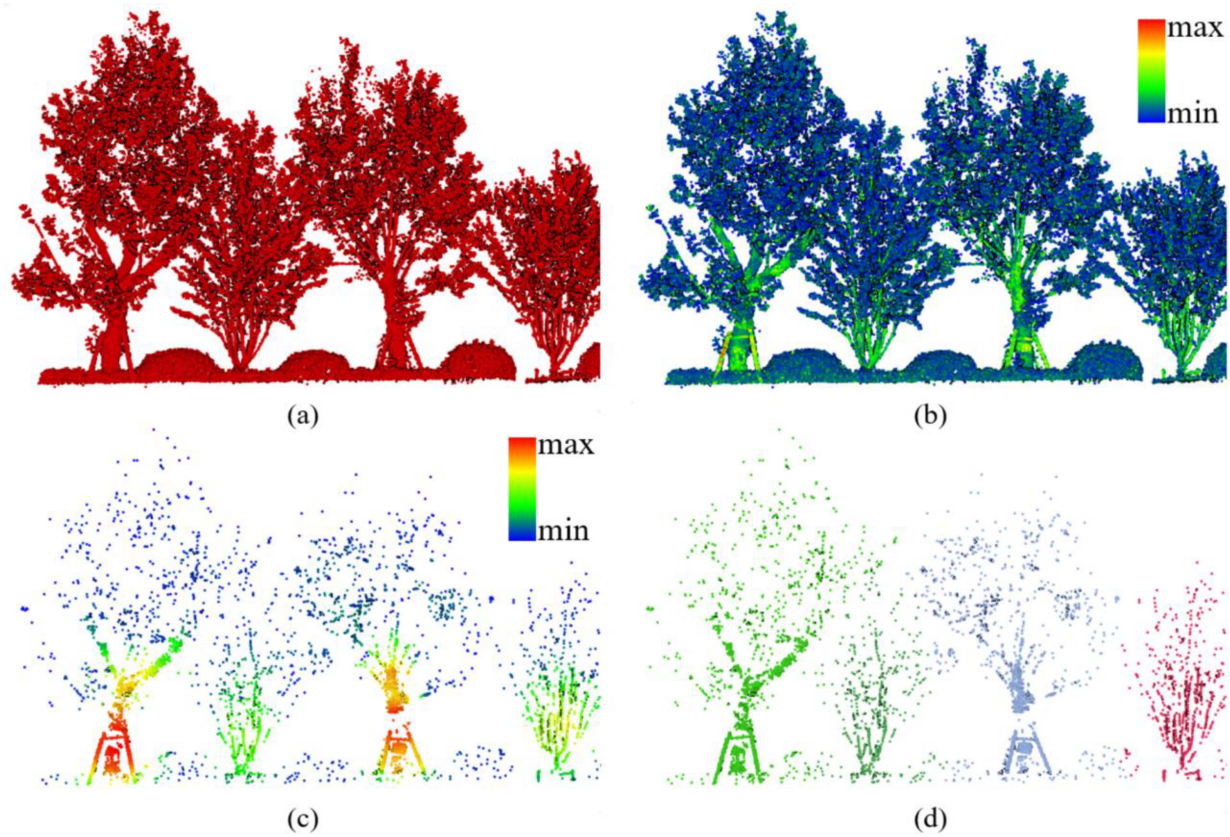

Fig. 5. Street tree nonphotosynthetic components clustering. (a) ROI including street trees. (b) Reflectance intensity distribution of ROI. (c) Nonphotosynthetic components colored by density. (d) Clustered nonphotosynthetic components (distinguished by colors).

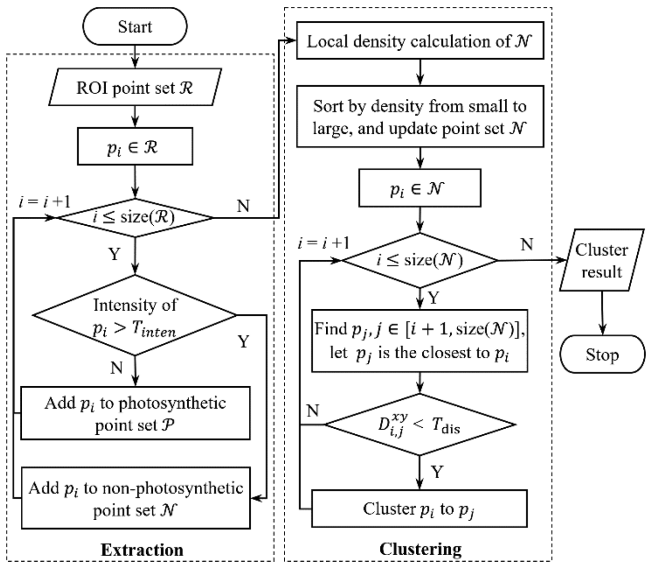

Fig. 6. Detailed process of extraction and clustering of nonphotosynthetic components.

of the tree points on each slice. After slicing, take the center of the bounding box with the smallest length among all slices as the center of the cylinder top surface, and take half of this bounding box length as the radius to establish a cylinder to cut the tree points below this slice [as slice i shown in Fig. 8(a)]. The points inside the cylinder are retained and the points outside the cylinder are deleted. Fig. 8(b) shows the first nontree points removal result. Then, starting from the top surface of the cylinder determined last time, slice down along the Z-axis and detect the non-tree points that meet the removal conditions again. This process is iterated until no point is removed. The individual segmentation results of each tree after gradual refinement are shown in Fig. 7(b), in which the understory vegetation and the trunk holders can be well removed.

Some nontree column pole-like objects (see Fig. 9) may exist in the segmented tree individuals due to insufficient removal in the ROI selection. After refinement by iterative slicing [see Fig. 9(d)], these individual pole-like objects appear markedly distinct from street trees with significantly smaller bounding box sizes. Therefore, we select and remove these nontree pole-like objects according to their spatial size to further refine the separated individuals.

To ensure the integrity of the extracted individual trees, we finally check and complete the tree trunks in the extracted results. In the ROI selection, we regard the vertical poles with a certain height as artificial and remove them, which may also include some tall and straight tree trunks. Therefore, some individual trees extracted from the ROI may lack trunks, as shown in Fig. 10. Therefore, we select the missing trunks from the artificial vertical poles based on the extracted individual trees (crowns). Specifically, the thinnest position found by iterative slicing is taken as the position of each tree to find the vertical

Fig. 7. Individual segmentation of street trees. (a) Clustering of photosynthetic components. (b) Street tree individual extraction result.

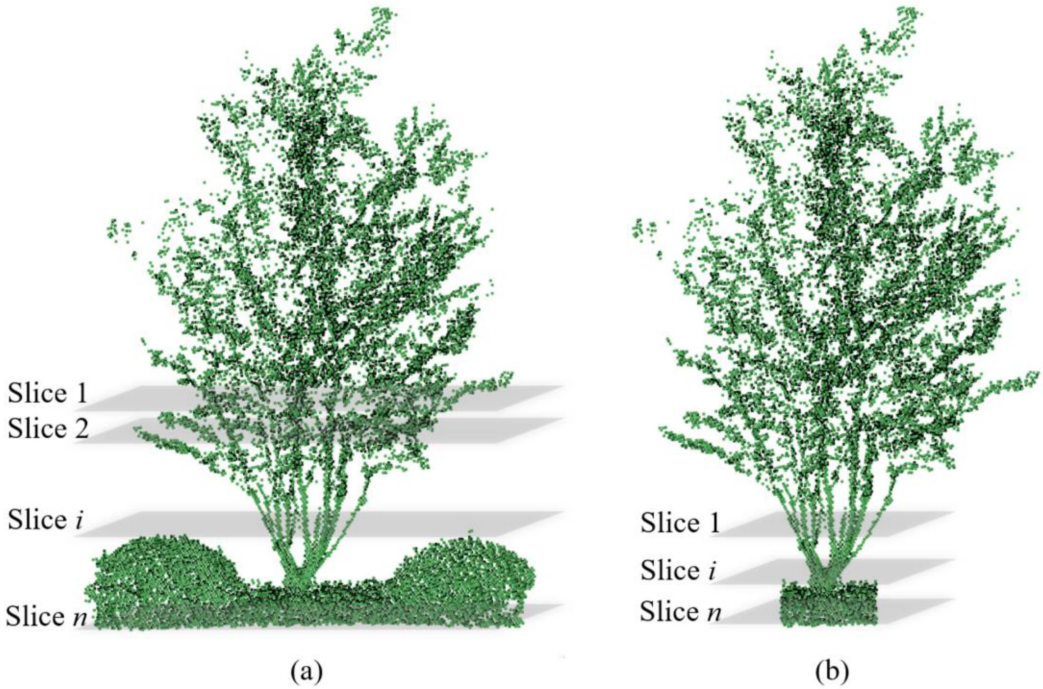

Fig. 8. Gradually removal of nontree components by iterative slicing. (a) First slicing. (b) Second slicing.

pole that is closest to it in horizontal. If the horizontal distance is less than the given threshold (such as 0.5 m), the found vertical pole is regarded as the trunk of this tree.

So far, complete segmentation of individual street trees can be realized.

III. Experiments and Evaluations

A. Experimental Data

The point cloud of an urban area shown in Fig. 11 is used to verify the feasibility and effectiveness of the proposed method. This data is obtained by a mobile laser scanning system equipped with RIEGL VUX-1UAV. This experimental area includes 6 roads with a total road length of about 2180 m and a total number of scanning points of 95 283 454. The average spacing between adjacent scanning points is about 3.1 cm. Different roads have different scene complexity, and most roads have two or more rows of trees on each side.

As for the first row of street trees on each side close to the road centerline, although most of the street trees on Road 1 have trunk holders, these trees are small, the spacing between adjacent trees is large, and the boundaries between tree crowns and artificial pole-like objects (e.g., street lights and traffic signs) are obvious, so they belong to simple common Scene 1. As there are many vehicles parked on the roadside of Road 2, most of the tree trunks on this road have different degrees of occlusion. Compared with Road 1, the street trees on Road 2 are larger, and there are overlaps between some tree crowns. Street trees on this

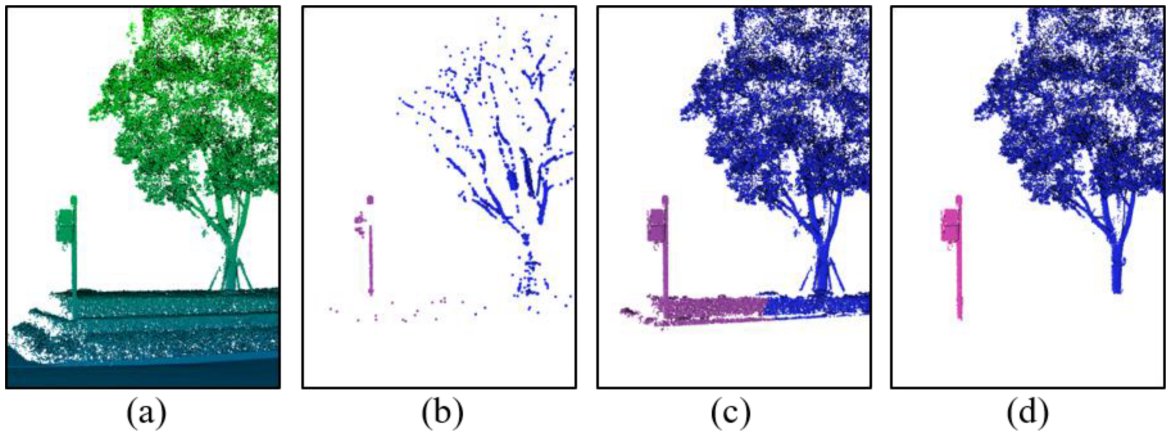

Fig. 9. Nontree column pole-like objects identification and optimization. (a) Raw points. (b) Nonphotosynthetic components clustering. (c) Clustering of photosynthetic components. (d) Refinement through iterative slicing.

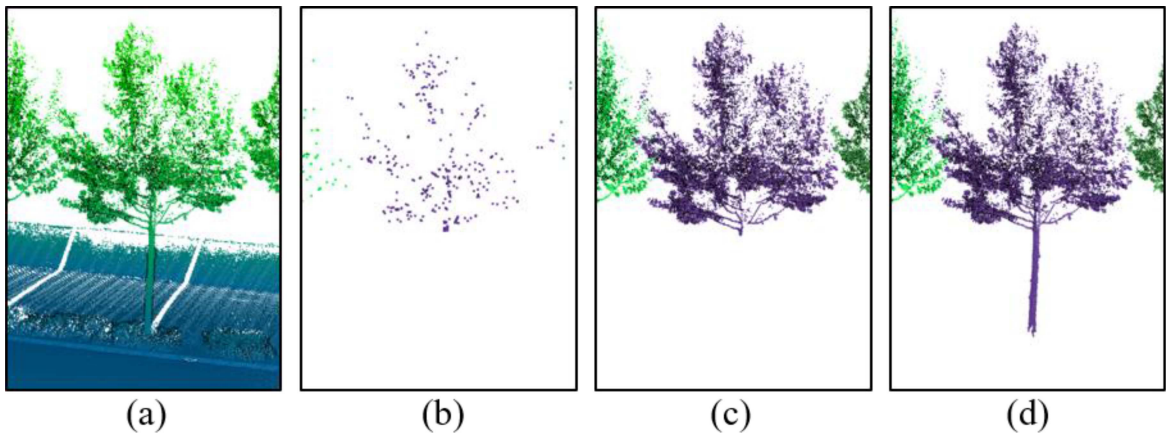

Fig. 10. Tree trunk completion. (a) Raw points. (b) Nonphotosynthetic components clustering. (c) Individual segmentation of street trees. (d) Result after trunk completion.

road belong to common Scene 3. The street trees on Road 3 are similar to those on Road 1, with large spacing between trees and little overlap with artificial poles, and there is no trunk holder on this road. The street trees on Road 4 are large, with serious overlap between tree crowns. Some street lights are seriously mixed in the tree crowns, and the tree trunks are similar to the artificial vertical poles. Therefore, street trees on this road belong to common Scene 2. Street trees on Road 5 are similar to those on Road 1 and Road 3, belonging to simple common Scene 1. The street trees on Road 6 are the most complex. Adjacent trees have different shapes and sizes, and there are serious overlaps between adjacent tree crowns. Some trees do not have obvious trunks, and even those with obvious trunks still have trunk holders. In addition, the understory vegetation is high and irregular, which seriously blocks the trunk. These trees belong to the most complex common street tree Scene 4.

Blocked by the first row of street trees near the road center, other trees on each roadside have different degrees of data missing. In addition, compared with the first row of trees, these trees are more different in type, shape, and spacing, which makes them similar to common street tree Scene 4. Although there are few artificial poles in these trees, it is still difficult to segment them accurately.

Different roads and street tree scenes in the experimental area can effectively verify the street tree individual extraction effect of the proposed method.

B. Experimental Process

Taking the road as the unit, we individually extract the street trees on each road in the experimental area.

First, the ground and buildings in the raw data are removed through data preprocessing. The experimental parameters and their values involved in this process are the same as those of Li et al. [22].

Then, the ROI that contain street trees and understory vegetation are selected. In this step, the length thresholds used to identify and remove artificial vertical and horizontal poles are taken as 4.5 m and 1.5 m, respectively, the distance threshold of Euclidean clustering is taken as 0.2 m, and the judgment threshold of the size of the ROI cluster is set to $3\,\mathrm{m} \times 3\,\mathrm{m} \times 3\,\mathrm{m}$. These experimental parameters are set according to the geometric characteristics of artificial poles and street trees in the experimental area.

After that, the nonphotosynthetic components of street trees are clustered. In this process, three empirically selected

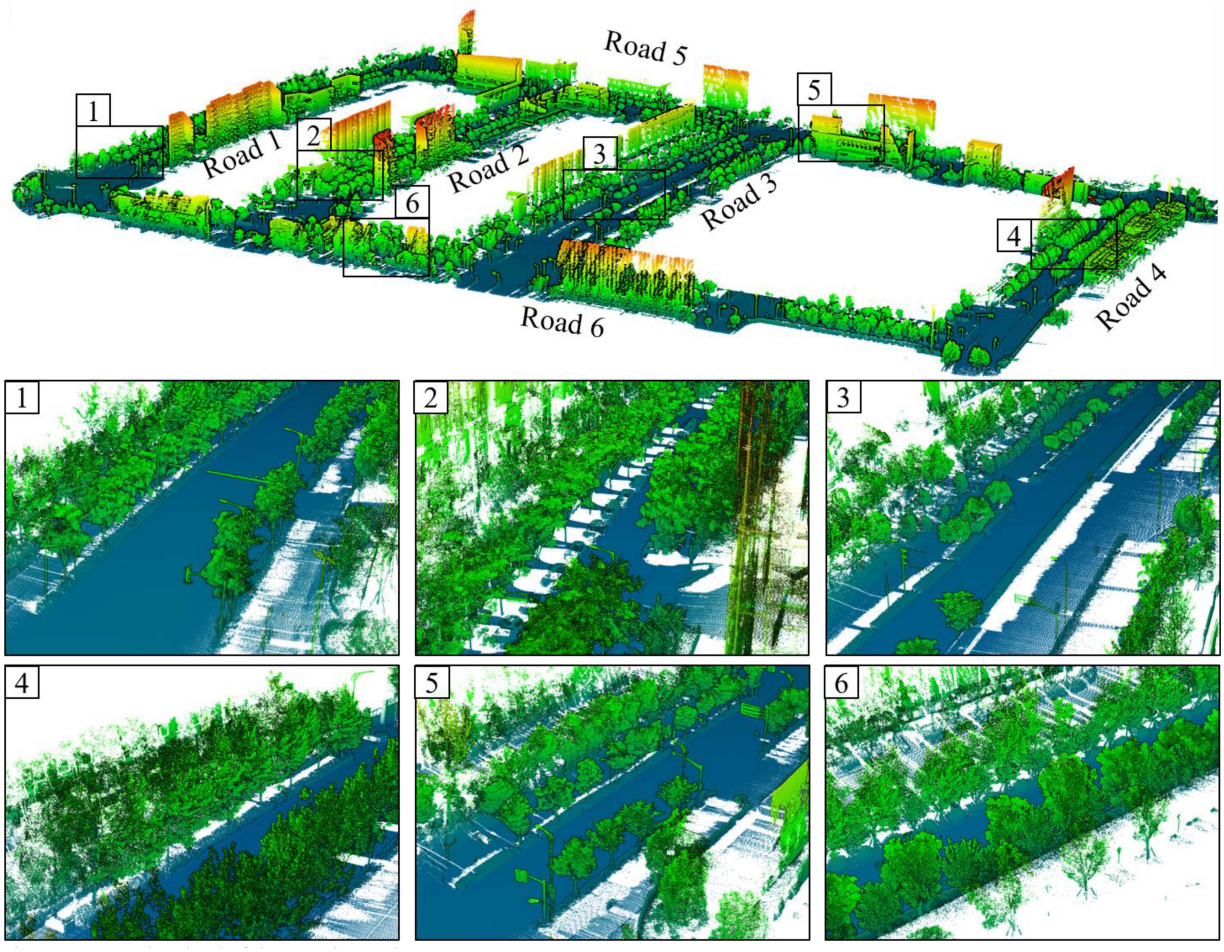

Fig. 11. MLS point cloud of the experimental area.

parameters are involved. The intensity threshold T_{inten} of selecting nonphotosynthetic component points is set to 20 000, the number of nearest neighbor points for calculating local density is taken as 50, and the horizontal distance threshold T_{dis} for clustering is taken as 2.0 m.

Finally, complete individual segmentation and refinement of street trees are realized. In this process, the threshold of space size in horizontal for nontree column pole-like objects recognition is set to $1\ \text{m} \times 1\ \text{m}$ and the threshold of horizontal distance for trunk completion is taken as 0.5 m according to their geometry.

Our proposed method is implemented in C++. The experiment is conducted on a computer with a 3.6 GHz CPU, 64 GB RAM, and a 64-bit Windows 10 operating system. The total time consumption for street trees individual extracting in the experimental area is approximately 125 min. Specifically, the time required for Road 1 to Road 6 is 19 min, 17 min, 14 min, 15 min, 27 min, and 33 min, respectively.

C. Evaluation Criterion

To quantitatively evaluate the extraction results, we calculated the precision P_r, recall R_e, and F-score f of the individual extraction of street trees. The precision and recall indicate the correctness and completeness of the extraction results, respectively, and F-score is an overall indicator that combines the two

$$\left.\begin{aligned} P_r &= \frac{\text{TP}}{\text{TP}+\text{FP}} \\ R_e &= \frac{\text{TP}}{\text{TP}+\text{FN}} \\ f &= \frac{2\times\text{TP}}{2\times\text{TP}+\text{FP}+\text{FN}} \end{aligned}\right\} \tag{5}$$

where TP represents the number of street trees that are correctly segmented and extracted, FP indicates the number of street trees that are wrongly segmented and extracted, and FN represents the number of street trees that have not been segmented and extracted. We divide the individual extraction results of a street tree into the following three cases. If the tree trunk in the raw data exists in the extraction result and more than 80% of the crown points are correctly segmented, this tree is considered to be correctly segmented and extracted. If the tree trunk in the raw data is missing in the extraction result or the crown points in the segmentation result are less than 80% of the original data, this tree is considered not to be extracted. If more than 20% of other tree points are mixed in the segmentation result or artificial objects that significantly affect the tree shape are mixed in the segmentation result, this tree is considered to be wrongly segmented and extracted.

TABLE I
QUANTITATIVE EVALUATION OF STREET TREE INDIVIDUAL EXTRACTION

Evaluation	Region													All
	Road 1_I	Road 1_O	Road 2_I	Road 2_O	Road 3_I	Road 3_O	Road 4_I	Road 5_I	Road 5_O	Road 6_I	Road 6_O	Road _I	Road _O	
TP	68	64	52	24	35	76	44	82	65	131	60	412	289	701
FP	1	6	1	1	0	15	0	0	5	11	1	13	28	41
FN	0	3	0	2	0	2	1	2	2	5	2	8	11	19
P_r (%)	98.6	91.4	98.1	96.0	100	83.5	83.5	100	92.9	92.3	98.4	96.9	91.2	94.5
R_e (%)	100	95.5	100	92.3	100	97.4	97.4	97.6	97.0	96.3	96.8	98.1	96.3	97.4
f (%)	99.3	93.4	99.0	94.1	100	89.9	89.9	98.8	94.9	94.2	97.6	97.5	93.7	95.9

I: Inner, O: Outer.

TABLE II
QUANTITATIVE EVALUATION OF STREET TREE INDIVIDUAL EXTRACTION IN DIFFERENT COMMON SCENES

Evaluation	Common street tree scene types and corresponding regions			
	Common Scene 1	Common Scene 2	Common Scene 3	Common Scene 4
	Road 1_I, Road 3_I, Road 5_I, Road 6_O	Road 4_I	Road 2_I, Road 2_O	Road 6_I, Road 1_O, Road 3_O, Road 5_O
TP	245	44	76	336
FP	2	0	2	37
FN	4	1	2	12
P_r (%)	99.2	100	97.4	90.1
R_e (%)	98.4	97.8	97.4	96.6
f (%)	98.8	98.9	97.4	93.2

I: Inner, O: Outer.

D. Experimental Results

The individual extraction results of street trees in the experimental area and some representative close-views are shown in Fig. 12. Fig. 13 shows some wrongly segmented and extracted street tree individuals. Among them, the segmentation result of the street tree in Fig. 13(a) contains traffic light which affects the crown shape, the trees in Fig. 13(b)–(f) are all under-segmented due to the influence of adjacent trees (too small and too close), and the trees in Fig. 13(g) and (h) are severely overlapped with the understory vegetation, resulting in the insufficient removal of these vegetation in the extraction results. Fig. 14 shows some street trees that have not been segmented and extracted. Most of these trees are too small to be detected when selecting the regions of interest or are removed incorrectly when removing the nontree column pole-like objects, as shown in Fig. 14(a), (b), (d), (f), and (h). The street tree individual extraction results in Fig. 14(c), (e), and (g) are all incomplete (lack of trunk or crown is oversegmented) due to the serious data occlusion.

We quantify the individual extraction results of street trees according to different road regions, as shown in Table I. Road _I refers to the first row of street trees on both sides of the road (i.e., inter street trees), and Road _O refers to other street trees on each road (outer street trees) except the first row. To avoid the serious data missing due to occlusion, only one row of trees closest to the road center except the first row on each road side is considered, and the trees located inside the fence are not included.

To evaluate the application effect of our method in common street tree scenes with different complexity, we classify the different road regions in the experimental area according to the common scenes, and calculate the individual extraction accuracy of street trees in different common scenes. The results are shown in Table II.

IV. DISCUSSION

A. Effectiveness of the Proposed Method

From the close-views of individual extraction of street trees on different roads in Fig. 12, it can be seen that benefiting from the effectiveness of street trees ROI selection based on supervoxels region growing, the individual extraction results of street trees are less affected by artificial pole-like objects such as street lights and traffic signs. The proposed nonphotosynthetic components clustering method based on intensity and density can well separate the main branch part of each tree. Although some leaf points are incorrectly identified as nonphotosynthetic components, it does not significantly affect the final individual extraction of the street trees. Since this method does not rely on the tree trunks to identify and locate street trees, although some trees do not have obvious trunks (e.g., some trees in the close-view of Road 3 and Road 6 in Fig. 12), or the trunk of some trees do not exist in the ROI due to their similarity to artificial vertical poles (e.g., some trees in the close-view of the clustered nonphotosynthetic components of Road 4 in Fig. 12), the location and contour of these trees can still be effectively separated, which allows these trees to be effectively identified and segmented in the final individual extraction results. The proposed individual tree segmentation and optimization method can effectively remove the nontree components especially the understory vegetation and artificial column pole-like objects. It can be seen from the close-views in Fig. 12 that for the high understory vegetation or trunk holders of some trees, although

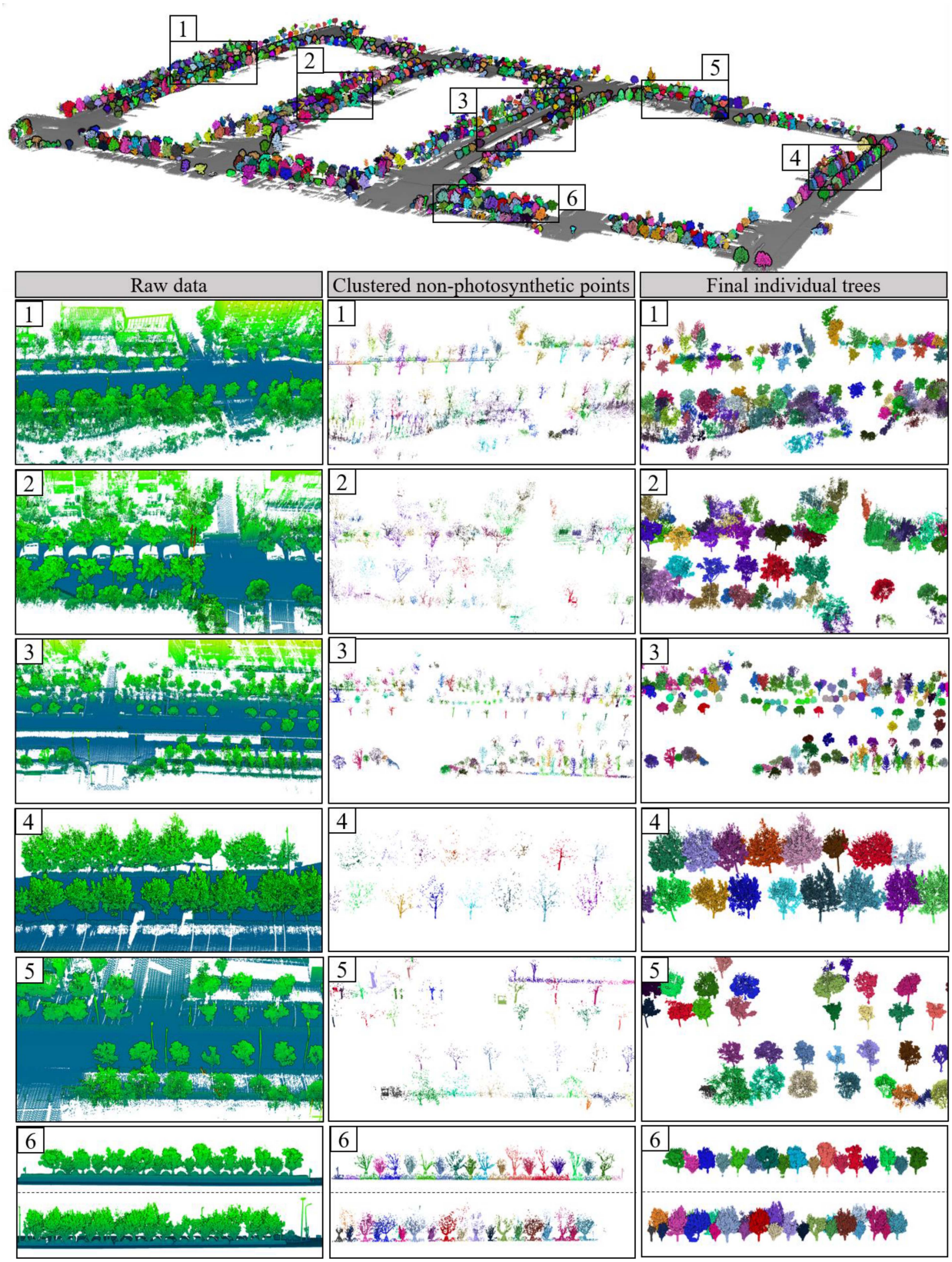

Fig. 12. Street tree individual extraction results and some representative close-views.

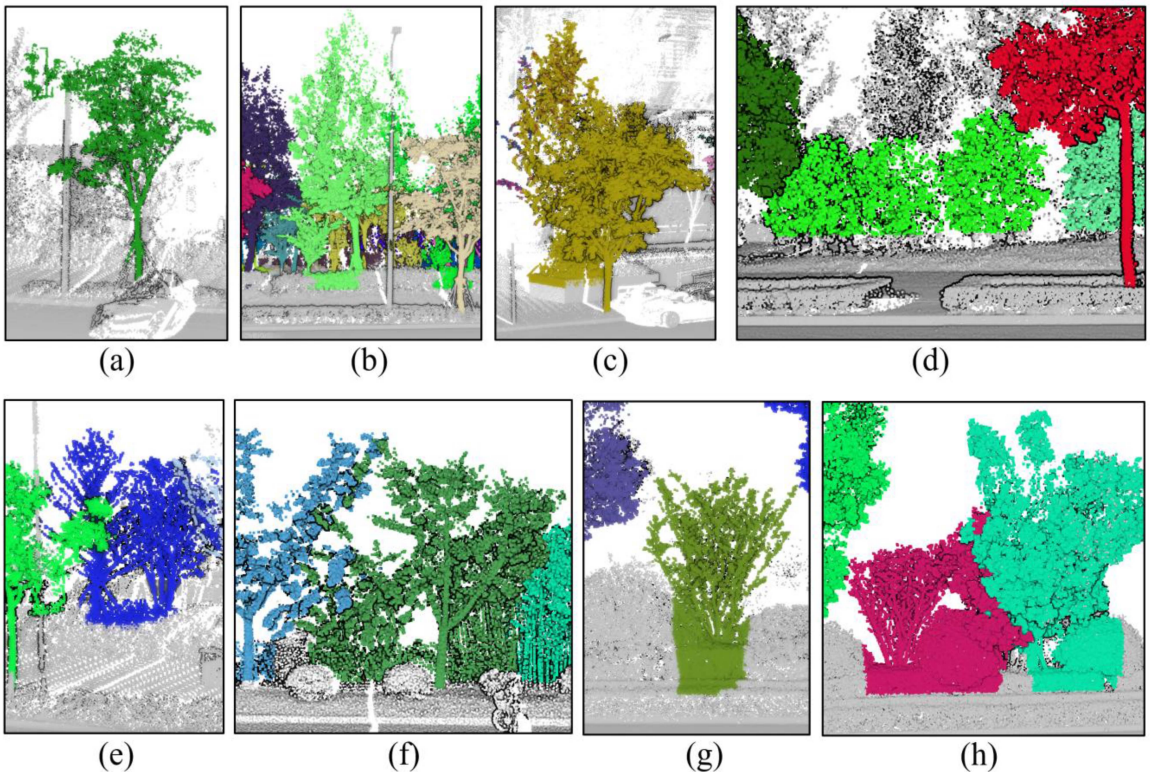

Fig. 13. Some wrongly segmented and extracted street trees. (a) Road 1_I; (b) road 1_O; (c) road 2_O; (d) road 3_O; (e) and (f): Road 5_O; (g) and (h): Road 6_I. (I: Inner, the first row of street trees on both sides of the road, O: Outer, other street trees on each road except the first row).

some of them exist in the clustered nonphotosynthetic components, these vegetation and trunk holders can be effectively removed in the final extracted individual trees. And for the short artificial column pole-like objects that exist in the ROI (e.g., close-view of Road 6 in Fig. 12), they can also be effectively removed in the final results. In addition, the missing tree trunks in the clustered nonphotosynthetic components (e.g., close-view of Road 4) can still be completed in the final individual tree extraction results.

As shown in the quantitative indicators presented in Tables I and II, our method achieves high accuracy in individual extraction of street trees for road scenes with varying complexity. Overall, the precision, recall, and F-score are 94.5%, 97.4%, and 95.9%, respectively. As for street trees in different road regions (inner and outer street trees), the extraction accuracy of the inner trees is higher than that of the outer. The overall precision, recall and F-score of the extraction of inner trees are 96.9%, 98.1%, and 97.5%, respectively. And the corresponding indicators for the outer street trees are 91.2%, 96.3%, and 93.7%, respectively. This is primarily due to the more regular shapes, sizes, and distribution patterns of inner street trees, as well as fewer instances of occlusion in the raw data. In terms of the common street tree scenes, our method can also achieve high-precision individual extraction of street trees in different common scenes. For simple common Scene 1, the precision, recall and F-score of the extraction are 99.2%, 98.4% and 98.8%, respectively. For the common Scene 2 with serious crown overlap, the corresponding three indicators are 100%, 97.8%, and 98.9%, respectively. And for the common Scene 3 with large data missing due to occlusion, these corresponding three indicators are all 97.4%. Even for the most complex common Scene 4, the extraction precision of our method reaches 90.1%, the recall is 96.6%, and the overall F-score reaches 93.2%.

As shown in Fig. 13, the typical wrongly extracted trees suggest that the primary reason affecting the precision of our individual extraction method is undersegmentation caused by adjacent small trees in close proximity. The spacing between these trees is too small, which is smaller than the clustering threshold we set in the nonphotosynthetic components clustering, so these trees cannot be correctly segmented [e.g., Fig. 13(b)–(f)]. In addition, our method cannot satisfactorily remove the understory vegetation overlapping with the tree crown (e.g., Fig. 13(g) and (h)). From the typical missed extracted trees in Fig. 14, the main reason that affects the extraction recall of our method is that the crown of some trees is too small. These trees are either undetected in the ROI selection or mistakenly deleted during the removal of nontree column pole-like objects [e.g., Fig. 14(a), (b), (d), (f), and (h)]. What is more, the incompleteness of extracted tree individuals caused by data missing due to occlusion is also one of the main factors that affects the recall of our method [e.g., Fig. 14(c), (e), and (g)].

B. Comparison With Existing Methods

To verify the advantages of our method, we compared our extraction accuracy with that of other existing methods, including Wu2013 [13], Wu2016 [14], Li2016 [15], Teo2016 [11], Zhong2017 [12], Xu2018 [6], Ning2022 [9], and Li2022 [17].

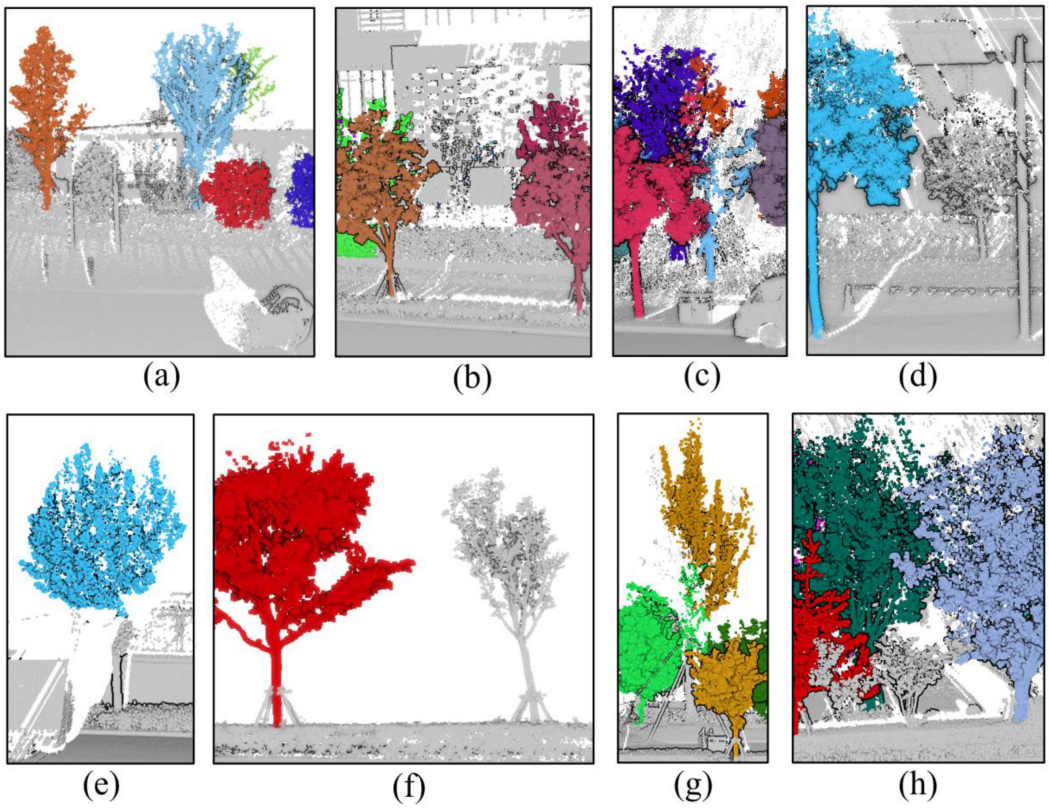

Fig. 14. Some street trees that have not been segmented and extracted. (a) and (b): Road 1_O; (c) and (d): Road 2_O; (e) road 4_I; (f) road 5_I; (g) road 5_O; (h) road 6_I. (I: Inner, the first row of street trees on both sides of the road, O: Outer, other street trees on each road except the first row).

TABLE III
COMPARISON OF STREET TREE INDIVIDUAL EXTRACTION BY DIFFERENT METHODS BASED ON MLS POINT CLOUDS

Method	Individual extraction strategy	Common street tree scene types	Number of trees	Tree types	P_r (%)	R_e (%)	f (%)
Wu2013 [13]	Bottom-up segmentation	Scene 1	140	Planetree and camphortree	100	99.3	99.6
Wu2016 [14]	Bottom-up segmentation	Scene 1	311	palmtree	89.0	86.2	87.6
Li2016 [15]	Bottom-up segmentation	Scene 1 Scene 3	66 29	mixed mixed	98.5 96.3	100 92.9	99.2 94.5
Teo2016 [11]	Top-down segmentation	Scene 1	804	-	100	96.0	98.0
Zhong2017 [12]	Top-down segmentation	Between Scene 1 and Scene 2	521	mixed	93.7	94.0	93.8
Xu2018 [6]	Classification based	Between Scene 1 and Scene 2	About 90	-	93.8	100	96.0
Ning2022 [9]	Classification based	Between Scene 1 and Scene 2	About 46	-	98.3	98.3	98.3
Li2022 [17]	Bottom-up segmentation	Scene 2	138	Planetree and camphortree	99.3	99.3	99.3
Proposed	Bottom-up segmentation	Scene 1 Scene 2 Scene 3 Scene 4	251 45 80 385	mixed mixed mixed mixed	99.2 100 97.4 90.1	98.4 97.8 97.4 96.6	98.8 98.9 97.4 93.2

Since the individual extraction results of street trees are highly related to the complexity of the scene where they are located, for objective comparison, we map the scene type of each study to the four common scenes defined in this article according to the street tree scene complexity presented in it. Among them, although there is some overlap between the adjacent crowns in the experimental scenes of Zhong2017 [12], Xu2018 [6], and Ning2022 [9], the overlap between tree crowns and the artificial pole-like objects is small, so they are divided into scenes between common Scene 1 and Scene 2. Table III shows the detailed comparison results.

It can be seen from the comparison results in Table III that most of the experimental scenes corresponding to the methods with a comprehensive accuracy F-score of more than 98% are relatively simple common Scene 1 and Scene 2, such as Wu2013 [13], Li2016_Scene1 [15], Teo2016 [11], Ning2022

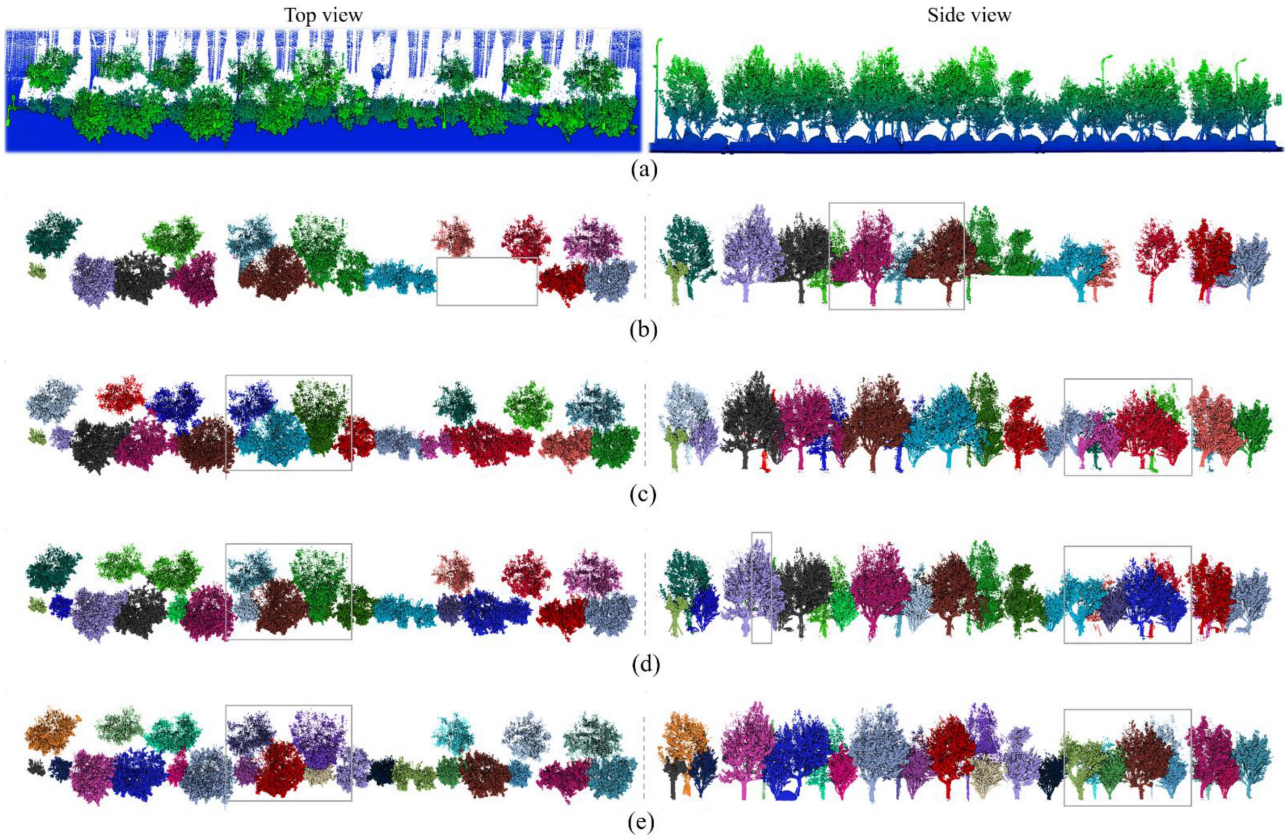

Fig. 15. Comparison of street tree individual extraction by different methods on complex common scenes.

[9], Li2022 [17], and ours on common Scene 1 and Scene 2. Even though there are small differences between the specific accuracy indicators of different methods (for example, the F-score of our method on common Scene 1 is 98.8% and Wu2013 [13] reaches the highest 99.6%), considering that the number of trees in the experimental area and the complexity of the scene are not identical, we believe that the extraction effects of these methods on simple scenes such as common Scene 1 and Scene 2 are equivalent and there is no significant difference. For common Scene 3 with trunk missing, according to Li2016_Scene3 [15], the method they proposed based on trunk detection and dual growing fails to detect trees without trunk points, resulting in the missing extraction of street trees in the final results. Therefore, the recall of this method is only 92.9%. Since our method does not rely on the detection of tree trunks, ours recall on common Scene 3 has reached 97.4%. In terms of the precision, there is no significant difference between the two methods, with precision of 96.3% and 97.4%, respectively.

For complex common Scene 4, according to Teo2016 [11] and Zhong2017 [12], their methods have the problems of missing extraction and inaccurate segmentation if there are understory vegetation and small trees, respectively. Therefore, both of them are not competent for common Scene 4 where there is dense vegetation under the trees and the tree sizes vary greatly. Among other methods for comparison, Wu2013 [13], Wu 2016 [14], and Li2016 [15] all use the trunk detection-based method to segment and extract individual trees, while Li2022 [17] identifies and locates each tree based on the junction of trunk and branches, and Xu2018 [6] and Ning2022 [9] both use treetops as the basis for the individual segmentation of each tree after classification. Here, to compare the extraction results on complex common Scene 4, we select Wu2013 [13], Li2022 [17], and Xu2018 [6] as representative methods for street tree extraction based on trunk, trunk-branches junction, and treetop detection to individually segment and extract street trees in complex Road 6. Some comparison results with the proposed method are shown in Fig. 15, and the extraction accuracy is shown in Table IV. It can be seen that the method of detecting trunks at 1.2 m–1.4 m above the ground of Wu2013 [13] cannot identify small trees without obvious trunks, resulting in a recall of only 47.9%. In addition, due to crown touching, the crowns of some small trees that have not been located will be segmented onto adjacent trees, which affects the precision of segmentation and extraction of the located trees (only 62.4%). Compared to Wu 2013 [13], the method of Xu 2018 [6] can locate more trees, including some small trees, using the treetop detection, which improves the recall of individual tree extraction to 62.0% and the precision to 68.2%. Despite this, there are still many small trees located under large trees that cannot be accurately identified and segmented. The method of identifying trunk-branch junctions in Li2022 [17] can further improve the recognition rate of small trees. However, in the final segmentation results, some tree trunks are incomplete due to interference from trunk holders, resulting in a recall of only 73.7% (although the precision reaches 81.0%). Compared to

TABLE IV
COMPARISON OF DIFFERENT METHODS ON COMPLEX ROAD 6

Method	TP	FP	FN	P_r (%)	R_e (%)	f (%)
Wu2013 [13]	78	47	85	62.4	47.9	54.2
Xu2018 [6]	101	47	62	68.2	62.0	65.0
Li2022 [17]	132	31	47	81.0	73.7	77.2
Proposed	191	12	7	94.1	96.5	95.3

the above three methods, our tree detection and location method based on the clustering results of nonphotosynthetic components does not dependent on the characteristic positions such as tree trunks and treetops, and can distinguish more small trees without obvious trunks. In addition, the iterative slicing method for optimizing understory vegetation ensures the integrity of the tree trunks. The precision and recall of our method on complex Road 6 have reached 94.1% and 96.5%, respectively.

In summary, compared with the existing methods, our method can achieve the same accuracy as the existing methods in simple common scenes, and for complex scenes where tree types, sizes, and heights vary greatly, and there is dense understory vegetation, our method has significant advantages in extracting individual street trees.

V. CONCLUSION

In this article, a new method based on tree nonphotosynthetic components clustering is proposed to extract street trees individually from MLS point cloud data, the key steps of which include data preprocessing, regions of interest selection, street tree nonphotosynthetic components clustering, and street tree individual segmentation.

The experiment on an urban area consisting of 6 roads with different complex scenes demonstrated that: 1) by selecting the regions of interest based on supervoxels region growing, the artificial pole-like objects mixed in the tree crown can be effectively removed, which provides a basis for the accurate identification and segmentation of street tree individuals, 2) the proposed non-photosynthetic components clustering method based on intensity and density can well identify and segment the main branch part of each street tree, even small trees without obvious trunks and mixed in large trees can be truly identified and segmented, 3) the proposed complete individual tree segmentation method based on nonphotosynthetic components and gradual refinement can effectively segment tree individuals and remove the nontree components especially the understory dense vegetation and trunk holders. The main advantage of the proposed method is that it can be applied to different complex common street tree scenes. For scenes where there are different degrees of overlap between street trees and between street trees and artificial pole-like objects (common Scene 1 and Scene 2), the comprehensive index F-score of the proposed method for individual extraction of street trees exceeds 98%. For scenes with tree trunk missing due to occlusion (common Scene 3), the F-score also exceeds 97%. Even for complex scenes where the types, sizes, and heights of adjacent trees vary greatly, and there are overlaps between trees and high vegetation under trees (common Scene 4), the precision, recall and F-score of our method also reach 90.1%, 96.6%, and 93.2%, respectively.

However, the individual tree segmentation effect of our method needs to be further improved for scenes where the understory vegetation is too high to overlap with the upper tree crowns, which is the focus of our future research.

REFERENCES

[1] L. Ma, Y. Li, J. Li, C. Wang, R. Wang, and M. A. Chapman, "Mobile laser scanned point-clouds for road object detection and extraction: A review," *Remote Sens.*, vol. 10, no. 10, 2018, Art. no. 1531, doi: 10.3390/rs10101531.

[2] J. Li, X. Cheng, Z. Wu, and W. Guo, "An over-segmentation-based uphill clustering method for individual trees extraction in urban street areas from MLS data," *IEEE J. Sel. Topics Appl. Earth Observ. Remote Sens.*, vol. 14, pp. 2206–2221, Jan. 2021, doi: 10.1109/jstars.2021.3051653.

[3] S. Xia and R. Wang, "Facade separation in ground-based LiDAR point clouds based on edges and windows," *IEEE J. Sel. Topics Appl. Earth Observ. Remote Sens.*, vol. 12, no. 3, pp. 1041–1052, Mar. 2019, doi: 10.1109/jstars.2019.2897987.

[4] S. Xia, D. Chen, J. Peethambaran, P. Wang, and S. Xu, "Point cloud inversion: A novel approach for the localization of trees in forests from TLS data," *Remote Sens.*, vol. 13, no. 3, pp. 1–10, 2021, doi: 10.3390/rs13030338.

[5] S. Xia, C. Wang, F. Pan, X. Xi, H. Zeng, and H. Liu, "Detecting stems in dense and homogeneous forest using single-scan TLS," *Forests*, vol. 6, no. 11, pp. 3923–3945, 2015, doi: 10.3390/f6113923.

[6] S. Xu, N. Ye, S. Xu, and F. Zhu, "A supervoxel approach to the segmentation of individual trees from LiDAR point clouds," *Remote Sens. Lett.*, vol. 9, no. 6, pp. 515–523, 2018, doi: 10.1080/2150704x.2018.1444286.

[7] Y. Xu, Z. Sun, L. Hoegner, U. Stilla, and W. Yao, "Instance segmentation of trees in urban areas from MLS point clouds using supervoxel contexts and graph-based optimization," in *Proc. 10th Int. Assoc. Pattern Recognit. Workshop Pattern Recognit. Remote Sens.*, 2018, pp. 1–5, doi: 10.1109/prrs.2018.8486220.

[8] M. Weinmann, M. Weinmann, C. Mallet, and M. Brédif, "A classification-segmentation framework for the detection of individual trees in dense MMS point cloud data acquired in urban areas," *Remote Sens.*, vol. 9, no. 3, pp. 1–28, 2017, doi: 10.3390/rs9030277.

[9] X. Ning, Y. Ma, Y. Hou, Z. Lv, H. Jin, and Y. Wang, "Semantic segmentation guided coarse-to-fine detection of individual trees from MLS point clouds based on treetop points extraction and radius expansion," *Remote Sens.*, vol. 14, no. 19, 2022, Art. no. 4926, doi: 10.3390/rs14194926.

[10] H. Guan, Y. Yu, Z. Ji, J. Li, and Q. Zhang, "Deep learning-based tree classification using mobile LiDAR data," *Remote Sens. Lett.*, vol. 6, no. 11, pp. 864–873, 2015, doi: 10.1080/2150704x.2015.1088668.

[11] T.-A. Teo and C.-M. Chiu, "Pole-like road object detection from mobile LiDAR system using a coarse-to-fine approach," *IEEE J. Sel. Topics Appl. Earth Observ. Remote Sens.*, vol. 8, no. 10, pp. 4805–4818, Oct. 2015, doi: 10.1109/jstars.2015.2467160.

[12] L. Zhong, L. Cheng, H. Xu, Y. Wu, Y. Chen, and M. Li, "Segmentation of individual trees from TLS and MLS data," *IEEE J. Sel. Topics Appl. Earth Observ. Remote Sens.*, vol. 10, no. 2, pp. 774–787, Feb. 2017, doi: 10.1109/jstars.2016.2565519.

[13] B. Wu et al., "A voxel-based method for automated identification and morphological parameters estimation of individual street trees from mobile laser scanning data," *Remote Sens.*, vol. 5, no. 2, pp. 584–611, 2013, doi: 10.3390/rs5020584.

[14] W. F., C. Wen, and J. Li, "Automated extraction of urban trees from mobile LiDAR point clouds," in *Proc. 2nd Int. Soc. Photogrammetry Remote Sens. Int. Conf. Comput. Vis. Remote Sens.*, 2016, vol. 9901, pp. 159–164, doi: 10.1117/12.2234795.

[15] L. Li, D. Li, H. Zhu, and Y. Li, "A dual growing method for the automatic extraction of individual trees from mobile laser scanning data," *Int. Soc. Photogrammetry Remote Sens. J. Photogrammetry Remote Sens.*, vol. 120, pp. 37–52, 2016, doi: 10.1016/j.isprsjprs.2016.07.009.

[16] S. Xu, S. Xu, N. Ye, and F. Zhu, "Automatic extraction of street trees' non-photosynthetic components from MLS data," *Int. J. Appl. Earth Observ. Geoinformation*, vol. 69, pp. 64–77, 2018, doi: 10.1016/j.jag.2018.02.016.
[17] J. Li, X. Cheng, and Z. Xiao, "A branch-trunk-constrained hierarchical clustering method for street trees individual extraction from mobile laser scanning point clouds," *Measurement*, vol. 189, 2022, Art. no. 110440, doi: 10.1016/j.measurement.2021.110440.
[18] H. Luo, C. Chen, L. Fang, K. Khoshelham, and G. Shen, "MS-RRFSegNet: Multiscale regional relation feature segmentation network for semantic segmentation of urban scene point clouds," *IEEE Trans. Geosci. Remote Sens.*, vol. 58, no. 12, pp. 8301–8315, Dec. 2020, doi: 10.1109/tgrs.2020.2985695.
[19] M. Weinmann, B. Jutzi, S. Hinz, and C. Mallet, "Semantic point cloud interpretation based on optimal neighborhoods, relevant features and efficient classifiers," *Int. Soc. Photogrammetry Remote Sens. J. Photogrammetry Remote Sens.*, vol. 105, pp. 286–304, 2015, doi: 10.1016/j.isprsjprs.2015.01.016.
[20] J. Yang, Z. Kang, and P. H. Akwensi, "A skeleton-based hierarchical method for detecting 3-D pole-like objects from mobile LiDAR point clouds," *IEEE Geosci. Remote Sens. Lett.*, vol. 16, no. 5, pp. 801–805, May 2019, doi: 10.1109/lgrs.2018.2882694.
[21] Y. Yu, J. Li, H. Guan, C. Wang, and J. Yu, "Semiautomated extraction of street light poles from mobile LiDAR point-clouds," *IEEE Trans. Geosci. Remote Sens.*, vol. 53, no. 3, pp. 1374–1386, Mar. 2015, doi: 10.1109/tgrs.2014.2338915.
[22] J. Li and X. Cheng, "Supervoxel-based extraction and classification of pole-like objects from MLS point cloud data," *Opt. Laser Technol.*, vol. 146, 2022, Art. no. 107562, doi: 10.1016/j.optlastec.2021.107562.
[23] J. Demantké, C. Mallet, N. David, and B. Vallet, "Dimensionality based scale selection in 3D LiDAR point clouds," *Int. Arch. Photogrammetry, Remote Sens. Spatial Inf. Sci.*, vol. 38, pp. 97–102, 2012, doi: 10.5194/isprsarchives-xxxviii-5-w12-97-2011.
[24] X. Li, Y. Shang, B. Hua, R. Yu, and Y. He, "LiDAR intensity correction for road marking detection," *Opt. Lasers Eng.*, vol. 160, 2023, Art. no. 107240, doi: 10.1016/j.optlaseng.2022.107240.
[25] Y. Yu, J. Li, H. Guan, F. Jia, and C. Wang, "Learning hierarchical features for automated extraction of road markings from 3-D mobile LiDAR point clouds," *IEEE J. Sel. Topics Appl. Earth Observ. Remote Sens.*, vol. 8, no. 2, pp. 709–726, Feb. 2015, doi: 10.1109/jstars.2014.2347276.
[26] L. Yan, H. Liu, J. Tan, Z. Li, H. Xie, and C. Chen, "Scan line based road marking extraction from mobile LiDAR point clouds," *Sensors (Switzerland)*, vol. 16, no. 6, pp. 1–21, 2016, doi: 10.3390/s16060903.
[27] P. Huang, M. Cheng, Y. Chen, H. Luo, C. Wang, and J. Li, "Traffic sign occlusion detection using mobile laser scanning point clouds," *IEEE Trans. Intell. Transp. Syst.*, vol. 18, no. 9, pp. 2364–2376, Sep. 2017, doi: 10.1109/tits.2016.2639582.
[28] A. Asvadi, L. Garrote, C. Premebida, P. Peixoto, and U. J. Nunes, "ROBOT 2017: Third Iberian robotics conference," *Adv. Intell. Syst. Comput.*, vol. 694, pp. 475–486, 2017, doi: 10.1007/978-3-319-70836-2_39.
[29] C. Ye et al., "Robust lane extraction from MLS point clouds towards HD maps especially in curve road," *IEEE Trans. Intell. Transp. Syst.*, vol. 23, no. 2, pp. 1505–1518, Feb. 2022, doi: 10.1109/tits.2020.3028033.

Jintao Li received the B.S. degree in surveying and geoinformatics from Shandong University of Science and Technology, Qingdao, China, in 2018. He is currently working toward the Ph.D. degree in science and technology of surveying and mapping with the College of Surveying and Geo-Informatics, Tongji University, Shanghai, China.

His research interests include LiDAR data processing, mobile mapping, road scene perception, and digital twinning.

Hangbin Wu received the B.E. degree in surveying and mapping engineering and the Ph.D. degree in geodetic from Tongji University, Shanghai, China, in 2005 and 2010, respectively.

He is currently an Associate Professor with the College of Surveying and Geo-Informatics, Tongji University. He has contributed more than 50 publications on the topic of his research interests, which include the collection and processing of point clouds, high-definition maps for autonomous driving, and data mining from BIG navigation data.

Xiaolong Cheng received the B.S. degree in surveying and mapping engineering from Henan University of Urban Construction, Pingdingshan, China, in 2009, the M.S. degree in geodesy and survey engineering from Nanjing Tech University, Nanjing, China, in 2012, and the Ph.D. degree in photogrammetry and remote sensing from Tongji University, Shanghai, China, in 2017.

He is currently an Associate Professor with the College of Civil and Surveying and Mapping Engineering, Jiangxi University of Science and Technology, Ganzhou, China. His research interests include LiDAR data processing, multisource data fusion, and three-dimensional modeling.

Yuanhang Kong received the B.E. degree in surveying and mapping engineering in 2021 from the College of Surveying and Geo-Informatics, Tongji University, Shanghai, China, where he is currently working toward the Ph.D. degree in science and technology of surveying and mapping.

His research interests include deep learning, analysis of point cloud, and image processing.

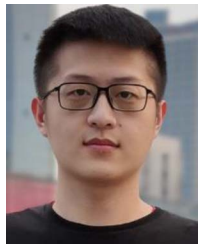

Xufei Wang received the B.S. degree in surveying and mapping engineering from Shandong Agricultural University, Taian, China, in 2019, and the M.S. degree in photogrammatry and remote sensing in 2022 from Tongji University, Shanghai, China, where he is currently working toward the Ph.D. degree in intelligent science and technology.

His research interests include point cloud processing, multisource data fusion, and simultaneous localization and mapping.

Yanyi Li received the B.E. degree in surveying and mapping engineering from the College of Geodesy and Geomatics, Shandong University of Science and Technology, Qingdao, China, in 2021. He is currently working toward the M.S. degree in science and technology of surveying and mapping with Tongji University, Shanghai, China.

His research interests include remote sensing technology and data processing.

Chun Liu (Member, IEEE) received the Ph.D. degree in geodesy and surveying from Tongji University, Shanghai, China, in 2001.

From 2001 to 2003, he was a Visiting Scholar with the Development of Infrastructure for Cyber Hong Kong, The Hong Kong Polytechnic University, Hong Kong. From 2007 to 2008, he was a Senior Visiting Scholar with the Laboratory of Mapping and Geographic Information Systems, The Ohio State University, Columbus, OH, USA. In 2011, he was a Senior Visiting Scholar with the Institute of Spatial Geodesy and Engineering Survey, University of Nottingham, Nottingham, U.K. He is currently a Full Professor of cartography and geography information engineering with the College of Surveying and Geo-Informatics, Tongji University. His research interests include multisource point cloud coupled semantic cognition and spatial–temporal smart sensing.